# Clean and pyrrole-functionalized Si- and C-terminated SiC surfaces: First-principles calculations of geometry and energetics compared with LEED and XPS

M. Preuss* and F. Bechstedt
*Institut für Festkörpertheorie und -optik, Friedrich-Schiller-Universität, Max-Wien-Platz 1, 07743 Jena, Germany*

W. G. Schmidt
*Theoretische Physik, Universität Paderborn, Warburger Straße 100, 33100 Paderborn, Germany*

J. Sochos, B. Schröter, and W. Richter
*Institut für Festkörperphysik, Friedrich-Schiller-Universität, Max-Wien-Platz 1, 07743 Jena, Germany*
(Received 29 June 2006; revised manuscript received 18 September 2006; published 5 December 2006)

The adsorption of pyrrole ($C_4H_5N$) on SiC(111)/(0001) and SiC($\overline{111}$)/(000$\overline{1}$) surfaces is studied by means of low-energy electron diffraction and x-ray photoelectron spectroscopy. Accompanying *first-principles* calculations of energies, geometries, and core-level shifts elucidate possible bonding geometries in dependence on the polarity and the reconstruction of the clean SiC surface. Models for the $\sqrt{3}\times\sqrt{3}$ and $3\times3$ phases of SiC($\overline{111}$)/(000$\overline{1}$) surfaces are presented and discussed.

DOI: 10.1103/PhysRevB.74.235406 PACS number(s): 79.60.−i, 68.43.Bc, 68.03.Hj

## I. INTRODUCTION

During the last years, the formation of organic thin films on crystal surfaces has attracted much attention in the surface science community, from both the fundamental and practical points of view.[1–3] In particular, organic functionalization is becoming an indispensable tool for the development of semiconductor-based devices. This technique comprises, on the one hand, the possibility to overcome the size limitations inherent to current-day silicon-based transistors by contacting source and drain with a (mono)molecular gate. On the other hand, it may be used for imparting molecular functionality onto inorganic components by, e.g., covalent immobilization, thus obtaining sensitivity towards chemical stimuli. If such hybrid systems are to be used, however, as highly selective sensors *in vivo*, nontoxicity in the living organism must be assured, which leads to the minimal demand of biocompatibility.[4]

Silicon carbide (SiC) is a promising candidate for such applications because it is mechanically extremely stable and indeed biocompatible. Its high breakdown field, high thermal conductivity, and strong bonding may turn out advantageously for high-power and high-frequency devices being operational up to 1000 K. The electronic properties of SiC can be tailored due to the large number of possible polytypes simply by variation of the SiC bilayer stacking along the [111] or [0001] direction. For example, the fundamental gap ranges from 2.4 eV in cubic 3C-SiC to 3.3 eV in hexagonal 2H-SiC.[5] The difficulties in the preparation procedure of clean, high-quality SiC crystals and surfaces have prevented its widespread commercial use by now. However, in this respect substantial progress has been made recently.[6]

The pyrrole [$C_4H_5N$, Fig. 1(a)] molecule has been chosen for organic functionalization of SiC surfaces for three reasons: first, it is a small aromatic molecule, resulting in a relatively limited number of conceivable bonding possibilities on SiC, contrary to, e.g., the adsorption of uracil on Si(001).[7] Second, it possesses as functional units a NH group and two carbon-carbon double bonds which may be used for further functionalization of the surface. Third, it is readily available in good quality, ensuring the reproducibility of the experimental results.

## II. EXPERIMENTAL METHODS

The experiments were performed in an ultrahigh-vacuum multichamber piece of equipment. The substrate preparation was similar as described in Refs. 8 and 9. The on-axis 6H-SiC (0001) polar surfaces (silicon or carbon face) were prepared *ex situ* by hydrogen etching at 1800 K. The nominally on-axis SiC surfaces show atomically flat terrraces up to several hundreds of nanometers wide. *In situ* substrate preparation was done by the common heating in Si flux to clean the surface and to obtain differently reconstructed substrate surfaces corresponding to different surface compositions. The stoichiometry and symmetry of the surfaces were controlled using low-energy electron diffraction (LEED), scanning tunneling microscopy (STM), and x-ray photoemission spectroscopy (XPS). The most stable structures on the Si-terminated surface appear in LEED images as $3\times3$, $(\sqrt{3}\times\sqrt{3})R30°$, and $(6\sqrt{3}\times6\sqrt{3})R30°$ patterns. They are characterized by about 1.3 and 1/3 additional Si adlayers on top of the bulk-terminated SiC and by a Si-depleted SiC surface

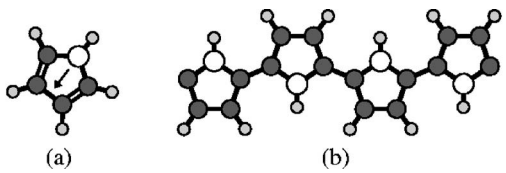


FIG. 1. (a) Sketch of the pyrrole molecule: white (gray, small gray) disks correspond to N (C, H) atoms, respectively, and double bonds are indicated; the permanent dipole moment ($\mu$=1.93 D) of the free molecule is represented by an arrow. (b) Part of a polypyrrole (PPy) chain.

 

lacking the upper Si layer, respectively. On the carbon face of SiC samples a $3\times3$ structure was observed. Pyrrole was vapor-deposited at substrate temperatures between 300 K and 1000 K in ultrahigh vacuum. Photoelectron spectra have been measured by Mg $K\alpha$ excitation at electron emission angles of 0° and 70° to the surface normal. The measured binding energies have been referenced to the silicon carbide signals of Si $2p$ at 100.8 eV and C $1s$ at 283.0 eV.

## III. COMPUTATIONAL METHODS

### A. Total energy calculations and modeling

The total energy and electronic structure calculations are performed using the gradient-corrected (PW91) (Ref. 10) density-functional theory (DFT) implemented in the Vienna *ab initio* simulation package (VASP).[11] The electron-ion interaction is described within the projector-augmented-wave scheme.[12] The electronic wave functions are expanded into plane waves up to an energy cutoff of 25 Ry, which has been demonstrated to be sufficient in our previous studies on small organic molecules in the gas phase[13] and adsorbed on Si(001).[14–16] The SiC surfaces are modeled with a periodically repeated slab where each supercell consists of six Si-C bilayers plus adsorbed pyrrole molecules and a vacuum region equivalent in thickness to 12 bilayers. Cubic stacking has been assumed along the (111) direction in each slab. Our previous calculations have shown that the actual stacking and, hence, the polytype of the substrate are of minor influence on the geometry and energetics of the surface layers.[17,18] The corresponding slab bottom layer is hydrogen saturated and kept frozen during the structure optimization whereas all other atoms are allowed to relax. The calculations are performed using the theoretical SiC equilibrium lattice constant of 4.387 Å. The residual minimization/direct inversion in the iterative subspace (RMM-DIIS) algorithm[19,20] is employed to minimize the total energy of the system. The molecular and surface atomic structure is considered to be in equilibrium when the Hellmann-Feynman forces are smaller than 10 meV/Å. The Brillouin zone integrations are carried out with four (eight) **k** points in its irreducible part in case of the $3\times3$ ($\sqrt{3}\times\sqrt{3}$) reconstructions.

### B. Surface core-level shifts

The core-level binding energy $E_b$ that is probed by XPS is, by definition, the energy that is necessary to remove a core electron from an atom. Formally it is given by the modified total energy difference

$$E_b = E(\mathrm{Z}(nl)-1) - E(\mathrm{Z}(nl)) - \varepsilon_F. \quad (1)$$

Here $E(\mathrm{Z}(nl))$ denotes the ground-state energy of the system where the core state of a certain atom of species Z is characterized by the quantum numbers $n$ and $l$. Correspondingly, $E(\mathrm{Z}(nl)-1)$ is the total energy of the system where one electron is removed from the $nl$ core state. The calculation of the binding energy according to Eq. (1) necessitates the sufficient localization of the excited hole in the core of the atom but this weak condition is practically always satisfied. Usually the binding energy $E_b$ is not measured with respect to the vacuum level, but with respect to the Fermi level $\varepsilon_F$ of the metallic sample holder.

In order to derive structural or chemical information about the system, the change of the binding energy due to the different environments of the considered atom, the core-level shift, is studied. In particular, the surface core-level shift (SCLS) is the difference between the core-level binding energies of an atom in a surface (surf) system and the same atom in a certain reference (ref) system [21]:

$$\mathrm{SCLS} \equiv \Delta S = E_b^{\mathrm{surf}} - E_b^{\mathrm{ref}}. \quad (2)$$

The screening of the core hole by the valence electrons describes the so-called final-state effects which, consequently, give rise to the so-called final-state surface core-level shift

$$\Delta S^{\mathrm{final}} = [E_{\mathrm{surf}}(\mathrm{Z}(nl)-1) - E_{\mathrm{surf}}(\mathrm{Z}(nl))] - \varepsilon_F^{\mathrm{surf}} - [E_{\mathrm{ref}}(\mathrm{Z}(nl)-1) - E_{\mathrm{ref}}(\mathrm{Z}(nl))] + \varepsilon_F^{\mathrm{ref}}. \quad (3)$$

The energies $E_{\mathrm{surf/ref}}$ include the full response of the system towards the core hole. In the explicit calculations the rearrangement of the core-electron density is neglected. If the screening of the core hole by the valence electrons is also discarded, i.e., by employing the frozen-orbital approach resulting in energies $\tilde{E}_{\mathrm{surf/ref}}(\mathrm{Z}(nl)-1)$, the total-energy differences in Eq. (3) reduce approximately to core-state eigenvalues $\varepsilon_c^{\mathrm{surf/ref}} = \tilde{E}_{\mathrm{surf/ref}}(\mathrm{Z}(nl)-1) - E_{\mathrm{surf/ref}}(\mathrm{Z}(nl))$ in accordance with Koopmans' theorem.[22] Within this so-called initial-state approximation we therefore calculate the initial-state surface core-level shifts as[23,24]

$$\Delta S^{\mathrm{ini}} = (\varepsilon_c^{\mathrm{surf}} - \varepsilon_F^{\mathrm{surf}}) - (\varepsilon_c^{\mathrm{ref}} - \varepsilon_F^{\mathrm{ref}}). \quad (4)$$

The necessary modifications to the DFT code in order to obtain access to the core-state energies $\varepsilon_c$ as well as to the energies $E(\mathrm{Z}(nl)-1)$ were implemented into VASP by Köhler and Kresse as described in Ref. 23.

We have concentrated on the nitrogen $1s$ (N $1s$) core level because nitrogen is not present on the clean surfaces and can therefore act as a direct probe for adsorbed molecules: if nitrogen is present in the XPS spectrum, then pyrrole adsorption has taken place. It is clear that the choice of the reference system is of crucial importance for values of the calculated SCLS. In this work we have examined three different systems. Isolated, gas-phase pyrrole (Py) suggests itself as the natural reference system because it is easy to calculate and, ideally, not influenced by hard-to-control interactions. Liquid pyrrole ($\ell$Py) might be closer to experimental conditions but is hard to simulate in DFT calculations. Here we have obtained a snapshot of liquid pyrrole from the following considerations: The bonding between the molecules in liquid pyrrole should be stronger than in the gas phase, but weaker than in a molecular solid. As a compromise, eight pyrrole molecules are put in a $10\times10\times10$ Å$^3$ supercell so that each occupies roughly 1/8 of the cube in which each one is aligned randomly in space. Also after full geometry optimization, no apparent order is observed so that the resulting structure is taken as a representative snapshot. Although this is a crude approximation to a liquid, we obtain an energy

gain of about 0.2 eV per molecule upon liquefaction compared to the gas phase and an average N 1*s* core-level energy comparable to the one of the isolated molecule. In this arrangement the density of the pyrrole liquid amounts to about 0.89 g cm$^{-3}$ compared to about 0.97 g cm$^{-3}$ under normal experimental conditions. This slightly diluted liquid should resemble the experimentally attainable reference system closely. Both the gas-phase and liquid reference systems have in common that the bonding between the molecules is weak so that the systems are stabilized by physisorption rather than by chemisorption. Polypyrrole (PPy), on the other hand, is a chain molecule with strong covalent bonds between the links, Fig. 1(b). Although the nitrogen atom is not involved in the covalent bonding, its chemical environment is changed so drastically that the calculated initial-state SCLS's are more than 1.5 eV larger than for the reference systems in which physisorption prevails as shown below. This indicates that even within the initial-state approximation the SCLS's are indeed sensitive to the chemical environment and that even subtle differences between seemingly similar reference systems show up in the values. It should be noted that the calculated SCLS's with respect to polypyrrole will be quoted for completeness rather than for an actual comparison to experimental values because polypyrrole was definitely not present during the measurements.

### C. Relation between adsorption energy and desorption temperature

To assess the stability of adsorption structures at experimental conditions it is possible to calculate approximate desorption temperatures from the adsorption energies which are equated to the height of the barrier that must be surmounted during the desorption process. The temperature-dependent desorption rate can be described by the Polanyi-Wigner equation[25,26]

$$k_{\mathrm{des}} = -\frac{\mathrm{d}N}{\mathrm{d}t} = \nu N^{\kappa} e^{-E_{\mathrm{a}}/k_{\mathrm{B}}T}, \tag{5}$$

where $N$ is the (temperature-dependent) number of molecules on the surface, $\kappa$ the desorption order, usually 0, 1, or 2, $E_{\mathrm{a}}$ the activation or barrier energy per molecule, and $\nu$ the frequency prefactor (in s$^{-1}$). Temperature-programmed desorption experiments are usually conducted employing a constant heating rate $\beta$ so that $T=T_0+\beta t$. The desorption of molecules from surfaces is a first-order process, so $\kappa=1$. The maximum desorption occurs for $\mathrm{d}k_{\mathrm{des}}/\mathrm{d}t=0$ which leads to the Randall-Wilkins expression[27]

$$\frac{E_{\mathrm{a}}}{k_{\mathrm{B}}T_{\mathrm{m}}^2} = \frac{\nu}{\beta} e^{-E_{\mathrm{a}}/k_{\mathrm{B}}T_{\mathrm{m}}}. \tag{6}$$

It can be rearranged into

$$T_{\mathrm{m}} = \frac{T_c}{\ln r - \ln \dfrac{T_c}{T_{\mathrm{m}}^2}} \equiv \frac{T_c}{\ln \dfrac{r}{r_0}}, \tag{7}$$

with $T_c=E_{\mathrm{a}}/k_{\mathrm{B}}$, $r=\nu/\beta$, and $r_0=T_c/T_{\mathrm{m}}^2$. This transcendental equation can be solved numerically for the temperature of maximal desorption, $T_{\mathrm{m}}$, with a given activation energy and plausible assumptions for the heating rate, $\beta\sim 1$ K s$^{-1}$, and for the frequency prefactor $\nu$. Consistent with the notion that desorption takes place by occupation of vibrational modes, $\nu$ is usually chosen between $10^{12}$ s$^{-1}$ and $10^{14}$ s$^{-1}$. The numerical solution of Eq. (7) with activation energies between 0 eV and 6 eV for fixed ratios $r$ reveals an approximately linear relationship (correlation coefficient 0.999) between activation energy and desorption temperature that is not unexpected because $r \gg r_0$ for typical values of $r\sim 10^{13}$ K$^{-1}$, $T_c = E_{\mathrm{a}}/k_{\mathrm{B}} \sim 10^4$ K, and $T_{\mathrm{m}}\sim 100$ K. If the explicit dependence of $r_0$ on the temperature $T_{\mathrm{m}}$ is neglected, $r_0$ (or $\ln r_0$, for that matter) can be regarded as a parameter and used in a least-squares fitting procedure. For ratios $r$ between $10^{12}$ K$^{-1}$ and $5.12\times 10^{14}$ K$^{-1}$ it varies linearly between $r_0=0.02013$ K$^{-1}$ and $r_0=0.02835$ K$^{-1}$. As one is mostly interested in a rough estimate for the desorption temperature it is sufficient to replace the varying $r_0$ by, e.g., the arithmetic mean of the maximal and minimal values. This results finally in the expression

$$T_{\mathrm{m}} = \frac{T_c}{\ln \dfrac{r}{0.02424\ \mathrm{K}^{-1}}}. \tag{8}$$

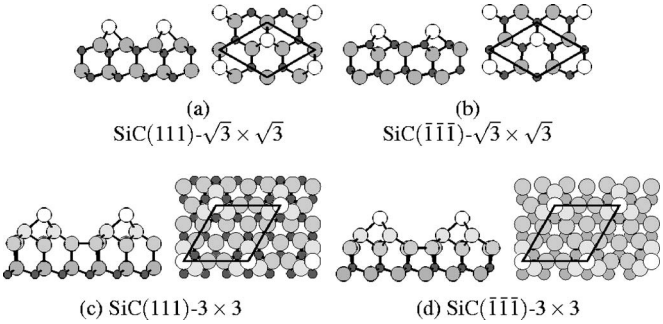


FIG. 2. Side and top views of the $\sqrt{3}\times\sqrt{3}$ [(a) and (b)] and $3\times 3$ [(c) and (d)] reconstructions of the Si-terminated SiC (111) and C-terminated SiC($\bar{1}\bar{1}\bar{1}$) surfaces studied here. Rhombohedral surface unit cells are indicated by solid lines. Si atoms are depicted as large circles with varying degrees of grayness, C atoms as small dark circles. The white Si adatoms are located in $T_4$ sites. In the $3\times 3$ reconstructions the Si trimer atoms on the additional full Si adlayer are found in threefold-coordinated hollow sites.

## IV. RESULTS: CLEAN SURFACES

To simplify the notation, the Si-terminated (111)/(0001) face of SiC will be denoted Si-SiC, the C-terminated ($\bar{1}\bar{1}\bar{1}$)/($000\bar{1}$) face C-SiC. Si-SiC is known to exhibit a variety of surface structures, the most prominent among them the $(\sqrt{3}\times\sqrt{3})R30°$ and the Si-rich $3\times 3$ reconstruction. The most stable $\sqrt{3}\times\sqrt{3}$ reconstruction over a wide range of preparation conditions consists of a Si adatom located in a effectively fourfold-coordinated site on top of an underlying second layer atom ($T_4$), Fig. 2(a).[28,29]

The Si-rich $3\times 3$ reconstruction contains a full Si adlayer complemented by a Si trimer and an additional Si adatom,

Fig. 2(c).[30,31] These geometries have been taken as a starting point for the calculation of the structural properties of the Si-SiC surfaces. The full geometry optimization yields bond lengths and bond angles which are in excellent agreement with previous experimental and theoretical investigations.

Unfortunately, to the best of our knowledge, there exist no models for the $3\times3$ and $\sqrt{3}\times\sqrt{3}$ reconstructions of the C face of SiC that are generally accepted, despite a large number of studies during the last decade.[32–36] Although the $\sqrt{3}\times\sqrt{3}$ phase on the C face is not observed in the experiments conducted in this work, we include in the calculations, for the sake of completeness, a model of C-SiC$(\sqrt{3}\times\sqrt{3})R30°$ consisting of a Si adatom in a $T_4$ site, Fig. 2(b), as suggested by Sabisch *et al.* in Ref. 28. In the case of the $3\times3$ phase of C-SiC we follow Hoster *et al.*[37] and employ a model for the $3\times3$ phase of C-SiC similar to the case of Si-SiC, Fig. 2(d): On top of the terminating carbon layer a Si wetting layer appears which is covered by the Si tetramer. The surface unit cell thus contains one dangling bond on the topmost Si adatom, in accordance with valence band emission spectra recorded by Li and Tsong.[38]

## V. RESULTS: PYRROLE-ADSORBED SURFACES

### A. Spectra, geometries, and coverage dependence

#### 1. X-ray photoelectron spectra

The x-ray photoelectron spectra of pyrrole on SiC(0001) obtained after different preparation steps revealed three different bonding states of N 1*s* electrons at binding energies of 400.3 eV, 399.6 eV, and 398.0 eV. The spectra corresponding to the latter two are shown in Fig. 3. The component at the highest binding energy (400.3 eV, not shown) was measured for a pyrrole film prepared by wetting a SiC surface in air with liquid pyrrole. That way, the N 1*s* signal of free or physisorbed pyrrole molecules is measured. The lower N 1*s* binding energy measured at 399.6 eV on pyrrole vapor-deposited in vacuum at room temperature can be assigned to a chemical bonding of the nitrogen atom to the silicon of the SiC substrate. This finding supports the model of NH dissociation and covalent attachment of pyrrole by N-Si bonding. After heating the samples of pyrrole adsorbed on SiC at a temperature higher than 600 K in vacuum, a third component at a lower binding energy of 398.0 eV was measured. The intensity of this component increases with temperature, and the signal at 399.6 eV disappears at 900 K. The low-binding-energy component can be assigned to silicon-nitride bonding due to decomposition of pyrrole at high temperature.

#### 2. Model geometries

Relaxed bonding geometries resulting from the calculations are depicted in Fig. 4 (see Fig. 5 for the definition of the tilt angle between molecule and surface normal). In the eight adsorption models studied here the starting geometry was that of the relaxed substrate structure plus one pyrrole molecule (save one H atom in the dissociated case) lying flat on the surface with the N atom about 1 Å away from the Si adatom. In this way it can be ensured that there is a substantial initial repulsive force acting on the atoms of the molecules that drives the structural optimization. The resulting Si-N distances are larger than 1 Å in all cases studied here (Table I). Neither for the choice of the initial pyrrole position nor during the structural relaxation any symmetry considerations or constraints having been employed, molecular as well as substrate atoms were completely free to relax. The computed key structural parameters are listed in Table I. The models have in common that the translational symmetry of the clean surface is kept; furthermore, in agreement with the LEED and XPS observations, the number of adsorbed pyrrole molecules is directly proportional to the number of dan-

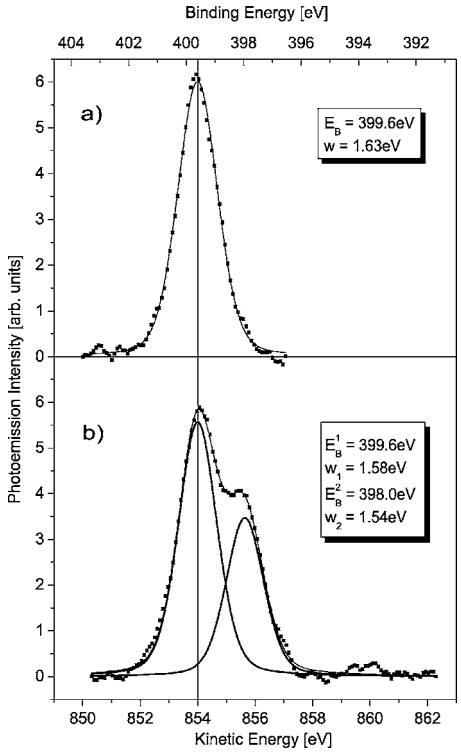


FIG. 3. Measured nitrogen 1*s* photoemission signals of pyrrole evaporated in vacuum at room temperature on 6H-SiC(0001) $-(\sqrt{3}\times\sqrt{3})R30°$ (a) before and (b) after heating in ultrahigh vacuum at 700 K. The peak positions on the binding-energy scale and the peak widths are given in the insets.

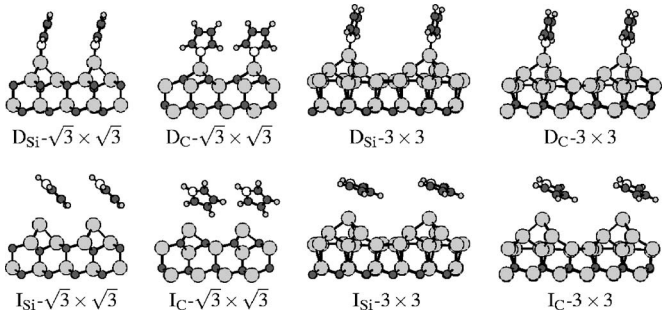


FIG. 4. Dissociated (*D*, upper row) and intact (*I*, lower row) adsorption structures of pyrrole on SiC surfaces with normals parallel to the bilayer stacking direction. The N atom of the five-membered pyrrole ring is rendered as a white circle, the C atoms as gray circles. The indices Si and C refer to the Si-face and C-face adsorption structures, respectively.

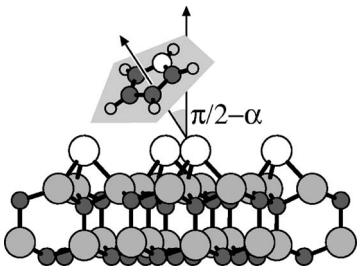


FIG. 5. Definition of the tilt angle $\alpha$ between the molecular plane and the SiC surface normal. White (gray, small gray) circles correspond to N (C, H) atoms, respectively, and large white and gray circles in the substrate represent Si atoms.

gling bonds. This observation limits the number of conceivable model geometries because it implies bonding of pyrrole at or near the surface adatom dangling bond.

### 3. Phase diagrams

For interfaces with different coverages, adsorption energies alone are not sufficient to assess the relative stability of the respective models. Here we simulate the experimental preparation conditions by taking into account the varying supplies of both hydrogen and pyrrole. Therefore we calculate the grand canonical potential $\Omega$ in dependence on the chemical potentials $\mu_P$ of pyrrole and $\mu_H$ of hydrogen,[39]

$$\Omega = F - n_P\mu_P - n_H\mu_H, \tag{9}$$

where $F$ is the free energy of the slab, and $n_P$ and $n_H$ are the numbers of pyrrole molecules and hydrogen atoms, respectively. Figure 6 indicates that the pyrrole-adsorbate structures can hardly be stabilized if the chemical potentials of hydrogen and pyrrole vary independently. Exemplarily we show the calculated two-dimensional phase diagram for the model structure $D_{Si}-\sqrt{3}\times\sqrt{3}$. The energy needed to dissociate a hydrogen atom from the pyrrole molecule amounts to about 2.8 eV so that pyrrole itself therefore acts as a hydrogen reservoir at ambient conditions. The phase diagram shows that over a wide range of hydrogen and pyrrole supplies the most favored pyrrole adsorption structure corresponds to full monolayer pyrrole coverage. The same observation is made for the other adsorption models studied here. This finding is in close agreement with a previous study of pyrrole adsorption on the Si(001) surface.[14]

TABLE I. Calculated key structural parameters of the pyrrole adsorbate structures. $\alpha$ corresponds to the tilt angle between the pyrrole molecular plane and the surface normal vector as defined in Fig. 5, N-Si denotes the nitrogen-silicon bond length, and $A\text{-}X_{T_i}$ $(i=1,2,3)$ the distance from the Si adatom to the nearest three substrate atoms ($X$=C for $D_C-\sqrt{3}\times\sqrt{3}$ and $I_C-\sqrt{3}\times\sqrt{3}$, else $X$=Si), and $A$-$X$ the corresponding distance on the clean reconstructed surface (all lengths in Å).

| Surface | $\alpha$ | N-Si | $A\text{-}X_{T_1}$ | $A\text{-}X_{T_2}$ | $A\text{-}X_{T_3}$ | $A$-$X$ |
|---|---|---|---|---|---|---|
| $D_{Si}-\sqrt{3}\times\sqrt{3}$ | 16.2° | 1.77 | 2.40 | 2.41 | 2.43 | 2.46 |
| $D_C-\sqrt{3}\times\sqrt{3}$ | 22.7° | 1.74 | 1.96 | 1.96 | 1.98 | 2.10 |
| $D_{Si}-3\times3$ | 12.2° | 1.78 | 2.40 | 2.42 | 2.45 | 2.52 |
| $D_C-3\times3$ | 10.2° | 1.76 | 2.38 | 2.41 | 2.42 | 2.56 |
| $I_{Si}-\sqrt{3}\times\sqrt{3}$ | 46.0° | 4.16 | 2.47 | 2.47 | 2.45 | 2.46 |
| $I_C-\sqrt{3}\times\sqrt{3}$ | 42.5° | 3.93 | 2.08 | 2.09 | 2.11 | 2.10 |
| $I_{Si}-3\times3$ | 68.6° | 3.48 | 2.46 | 2.47 | 2.49 | 2.52 |
| $I_C-3\times3$ | 60.5° | 3.54 | 2.54 | 2.55 | 2.58 | 2.55 |

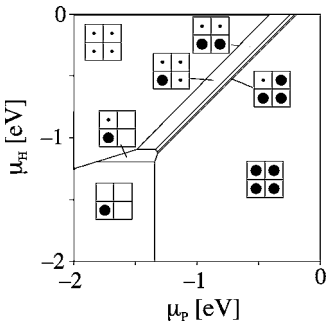


FIG. 6. Calculated phase diagram for the model structure $D_{Si}-\sqrt{3}\times\sqrt{3}$ (periodicity doubled in direction of the surface lattice vectors) in dependence on pyrrole ($\mu_P$) and hydrogen ($\mu_H$) chemical potential. Zero chemical potentials correspond to the free energies of an isolated pyrrole molecule and an isolated H atom, respectively. The square icons stylize the different adsorption phases seen from above: large black disk (●) pyrrole, black dot (·) hydrogen, and open square (□) free dangling bond.

The presentation proceeds as follows: We discuss the structural, energetic, and electronic properties of the model systems characterized by dissociative adsorption ($D$) in Sec. V B 1 and by molecular adsorption ($I$) in Sec. V B 2. In each respective section we begin with the $\sqrt{3}\times\sqrt{3}$ reconstructions and then turn to the $3\times3$ reconstructions.

## B. Structural, energetic, and electronic properties

### 1. Dissociated structures $D_{Si/C}-\sqrt{3}\times\sqrt{3}$ and $D_{Si/C}-3\times3$

The four relaxed $D$-interfaces are similar with respect to the N-Si bond length of about 1.76 Å which is characteristic for a covalent bond between nitrogen and silicon and thus confirms the experimental finding of a N-Si bond formation.

The dissociated pyrrole molecules are not exactly standing upright due to the influence of the nitrogen lone pair, but are only slightly tilted with respect to the surface normal with tilting angles $\alpha$ between 10.2° and 22.7°; see Table I and Fig. 4.

The most striking feature can be observed for the adsorbate structure $D_C-\sqrt{3}\times\sqrt{3}$. During the molecule adsorption the Si adatom is moved from its $T_4$ site into a $H_3$ site [see Fig. 2(b) and Fig. 4 for comparison]. As the symmetry change occurs spontaneously during the geometry optimization without any additional external fields or else, the pyrrole molecule obviously lowers the small energy barrier separating the $T_4$ and $H_3$ structures of the clean C-SiC$-\sqrt{3}\times\sqrt{3}$ surface. This result shows that the properties of the C face are remarkably different from those of the Si face although the starting overlayer configurations strongly resemble each other and should in principle exhibit the same chemistry. This different behavior may be related to a large extent to the

TABLE II. Calculated adsorption energies per molecule of full monolayer pyrrole/SiC interfaces, initial and final-state N 1*s* surface core-level shifts (SCLS's) with respect to liquid pyrrole ($\ell$Py), gas-phase pyrrole (Py), and polypyrrole (PPy).

| | | N 1*s* initial-state SCLS $\Delta S^{\text{ini}}$ (eV) | | | N 1*s* final-state SCLS $\Delta S^{\text{final}}$ (eV) | | |
|---|---|---|---|---|---|---|---|
| Surface | $E_{\text{ad}}$/eV | $\ell$Py | Py | PPy | $\ell$Py | Py | PPy |
| $D_{\text{Si}}-\sqrt{3}\times\sqrt{3}$ | 1.39 | 0.22 | 0.05 | 1.61 | −1.39 | −2.30 | −0.51 |
| $D_{\text{C}}-\sqrt{3}\times\sqrt{3}$ | 1.63 | 0.24 | 0.06 | 1.63 | −1.40 | −2.30 | −0.52 |
| $D_{\text{Si}}-3\times3$ | 3.18 | 0.25 | 0.08 | 1.64 | −1.66 | −2.57 | −0.78 |
| $D_{\text{C}}-3\times3$ | −0.11 | −0.54 | −0.71 | 0.85 | −1.64 | −2.55 | −0.76 |
| $I_{\text{Si}}-\sqrt{3}\times\sqrt{3}$ | 0.08 | −1.57 | −1.74 | −0.18 | −0.61 | −1.51 | 0.27 |
| $I_{\text{C}}-\sqrt{3}\times\sqrt{3}$ | 0.14 | −1.16 | −1.33 | 0.23 | −0.79 | −1.69 | 0.09 |
| $I_{\text{Si}}-3\times3$ | 2.14 | −1.06 | −1.23 | 0.33 | −0.75 | −1.66 | 0.13 |
| $I_{\text{C}}-3\times3$ | −0.87 | −1.21 | −1.38 | 0.18 | −0.71 | −1.61 | 0.17 |

different bond polarities of the Si-Si and Si-C bonds which influence the further attachment of molecules. This conjecture is corroborated by the observation that the *structural* differences between the C and Si faces are less pronounced for the $3\times3$ reconstruction where the additional Si layer reduces the effect of the terminating bilayer.

The *energetic* and *electronic* properties, however, differ drastically for the adsorption structures on the Si and C faces with $3\times3$ reconstructions. The $D_{\text{Si}}-3\times3$ model gives rise to a substantial adsorption energy of more than 3.0 eV, Table II, while the $D_{\text{C}}-3\times3$ model turns out to be unstable; i.e., the total energy of the interface system is higher than the sum of total energies of the substrate and adsorbate alone. Nevertheless, the geometry optimization finds that the dissociated molecule stays at the surface with a bonding between the Si adatom and the N atom which, judging from the bond length of 1.76 Å, has a covalent character. This structure corresponds to a local minimum on the total energy surface, so consequently there must exist an energy barrier for the detachment of the fragmented pyrrole which is even higher than 0.11 eV. Therefore this configuration, if realizable at all, is at best a transition state during the formation of ordered overlayers.

For the interpretation of the calculated SCLS's we restrict ourselves to the values obtained with respect to liquid pyrrole. This is justified because this reference system comes closest to what is realized in the XPS experiment; see the beginning of Sec. V. It is remarkable to note from Table II that the initial- and final-state SCLS's $\Delta S^{\text{ini}}$ and $\Delta S^{\text{final}}$ for the surface models $D_{\text{Si}}-\sqrt{3}\times\sqrt{3}$, $D_{\text{C}}-\sqrt{3}\times\sqrt{3}$, and $D_{\text{Si}}-3\times3$ are qualitatively different as they differ in sign. This fact suggests that the screening of the core hole in the N 1*s* state plays a major role in the adsorption pyrrole/SiC system, whereas the effect was shown to be of minor importance, e.g., for the Ga 3*d* state of relaxed GaAs(110) surfaces.[40] Although the obtained final-state SCLS's for all the four dissociated structures are, in absolute numbers, about twice as large as the experimentally determined shift of −0.7 eV for the $\sqrt{3}\times\sqrt{3}$ Si-face structure, they confirm the experimental observation that the Si-face as well as the C-face structures exhibit shifts with the same sign and in the same order of magnitude; from the x-ray photoelectron spectra of the latter (not shown), a likewise shift of −0.7 eV was derived. Moreover, anticipating the results for the intact adsorption geometries in Sec. V B 2, the trend of the final-state SCLS's is in accordance with the chemical intuition that atoms in a physisorbed molecular overlayer experience smaller shifts than when covalently attached to the surface. The initial-state SCLS's, however, would predict the largely counterintuitive reversed trend.

Thus from the SCLS's alone we cannot finally prove or disprove the models for the $\sqrt{3}\times\sqrt{3}$ and $3\times3$ C faces, but from the negative adsorption energy the (hypothetical) $D_{\text{C}}-3\times3$ model turns out to be unable to support a stable molecular overlayer, and indeed the $3\times3$ reconstruction vanishes on the C face after dosing with pyrrole.

#### 2. *Intact structures* $I_{\text{Si/C}}-\sqrt{3}\times\sqrt{3}$ *and* $I_{\text{Si/C}}-3\times3$

The adsorption models with intact pyrrole molecules (*I*) (see lower panel of Fig. 4 and Table I) vary in numbers and conceptually from the dissociated ones. The adsorption of the intact pyrrole molecules on the SiC substrates does not take place by covalent attachment, but by weak physisorption in the case of the models $I_{\text{Si}}-\sqrt{3}\times\sqrt{3}$ and $I_{\text{C}}-\sqrt{3}\times\sqrt{3}$ with adsorption energies of 0.08 eV (Si face) and 0.14 eV (C face) which are one order of magnitude smaller than those for the $D-\sqrt{3}\times\sqrt{3}$ models. These values correspond to desorption temperatures, as calculated from Eq. (8), of approximately 26 K (Si face) and 46 K (C face) which are way below the experimentally employed vapor-deposition temperatures. Thus at room temperature these structures are unlikely to appear in contrast to the dissociated pyrrole overlayers with high maximum desorption temperatures of about 470 K ($D_{\text{Si}}-\sqrt{3}\times\sqrt{3}$) and 520 K ($D_{\text{C}}-\sqrt{3}\times\sqrt{3}$).

The intact $\sqrt{3}\times\sqrt{3}$ as well as the intact $3\times3$ models have in common that the pyrrole molecule itself remains flat but assumes a geometry with a large tilting angle $\alpha$ and NH group far away from the surface (N-Si distances between 3.4 Å and 4.2 Å). That means that the actual weak attractive interaction takes place between the dangling bond of the Si atom and the lowest-lying CH group of pyrrole. Apart from this, they differ considerably. The model $I_{\text{C}}-\sqrt{3}\times\sqrt{3}$ stands out because the molecule adopts a position which can be imagined to be derived from $I_{\text{Si}}-\sqrt{3}\times\sqrt{3}$ by substitution of the substrate and a rotation of the adsorbate around a mo-

lecular in-plane axis. Although no symmetry change of the Si adatom occurs as in model $D_C-\sqrt{3}\times\sqrt{3}$, the situations are comparable because they show the drastic influence of the nominal surface termination on the molecular adsorption pathway due to the differences in bond polarities.

The intact pyrrole adsorption structures on the $3\times3$ reconstructed surfaces, on the other hand, are *structurally* similar to each other as is observed for the respective dissociated adsorption models whereas the *energetics* is found to be antipodal: we predict the $I_{Si}-3\times3$ model to be stable with an accompanying energy gain of 2.1 eV whereas the formation of the geometrically alike $I_C-3\times3$ model is strongly endothermic with a necessary energy expense of more than 0.8 eV. The relatively high adsorption energy of 2.1 eV for the $I_{Si}-3\times3$ model obviously contradicts the identification of this model as a physisorbed structure although the calculated N-Si distance of 3.48 Å is about twice as large as the sum of the covalent radii of N and Si. A possible explanation is that the main contribution to the adsorption energy arises not from the interaction between the adsorbate and the substrate, but from the intermolecular interaction of the pyrrole overlayer. It is stronger than in the intact $\sqrt{3}\times\sqrt{3}$ models because of the substantially larger tilting angle $\alpha$ of 68.6°. Apparently, the smaller tilting angle of 60.5° in the $I_C-3\times3$ model corresponds to a smaller lateral interaction that is not sufficient to lead to a positive adsorption energy.

Again, initial-state and final-state SCSL's predict contradicting trends. The initial-state SCLS's have large negative values $\Delta S^{ini}$ of the order of −1.5 eV that indicate a strong change of the atomic nitrogen potential upon intact molecular adsorption, although with respect to liquid pyrrole one expects these changes to be small because the chemical environment of the corresponding nitrogen atom is, at least in an atomic picture, very similar both in the adsorbate and in the reference system. Nevertheless, the final-state SCLS's of the order of −0.7 eV show that there is indeed a change of the chemical environment but which is less pronounced than in the case of the dissociated adsorption geometries: the SCLS's for the *I* models are smaller by a factor of 2 than for the *D* models. From the comparison of final-state SCLS's to the experimental shift of −0.7 eV one could be tempted to conclude that the intact adsorption geometries are the ones that are realized in the experiments. However, this interpretation falls short of taking into account the systematically lower adsorption energies of the *I* models (with the exception of $I_{Si}-3\times3$) that hamper their occurrence at the experimental preparation temperatures; see the beginning of this section. Considering the uncertainties of the theoretical models the calculated SCLS's are in any case to be interpreted with due caution. Moreover, even the final-state approximation employed here does not include the possible rearrangement of the remaining core electrons.

Especially for the N 1*s* state this effect is expected to lead to a substantial change in the core-level shifts because the extraction of one of the two *s* electrons strongly modifies the character of the state. In the case of the Ga 3*d* state, mentioned in Sec. V B 1, the emission of one of the ten *d* electrons should alter the state only slightly. Therefore the shifts alone are not sufficient to obtain a final decision on the realized adsorption geometries.

## VI. SUMMARY AND CONCLUSIONS

The adsorption of pyrrole on the Si and C faces of the $\sqrt{3}\times\sqrt{3}$ and $3\times3$ reconstructed SiC(111)/(0001) surfaces has been studied experimentally by LEED and XPS and theoretically by *ab initio* calculations of structure, energetics, and surface core-level shifts. The calculations elucidate two major reaction pathways: NH dissociation (*D*) and covalent attachment of pyrrole upon adsorption and physisorption (*I*) of the nondissociated molecule. The dissociative adsorption is found to be favored both from the calculations and from the experimental findings. Pronounced differences between the *D* and *I* pathways are, above the geometry distinction, the systematically lower adsorption energies of the latter which render their realization improbable at ambient conditions. Furthermore, the calculated final-state SCLS's with respect to liquid pyrrole differ by about a factor of 2. The corresponding initial-state SCLS's, however, not only show a large scatter in the values, but also magnitudes which apparently contradict expectations from a chemistry point of view, and they seemingly predict different directions of the shift for the first three dissociated models and the intact models. For both the initial- and final-state SCLS's the deviations are traced back to the drastic changes the N 1*s* state experiences upon extraction of a core electron which are not covered in either of these approaches to the calculation of surface core-level shifts.

While the geometries of the clean Si-face of SiC(0001) or SiC(111) with $\sqrt{3}\times\sqrt{3}$ or $3\times3$ translational symmetries are well established and agreed upon, no such models exist for the corresponding C faces. One partial aim of this study was to use pyrrole to probe the surface composition of the $3\times3$ phase of the C face: the x-ray photoemission spectra hinted at the formation of a covalent N-Si bond and, as such, to the presence of Si at the C face. The proposed adlayer-adtrimer-adatom model was sufficient to explain the instability of an ordered overlayer of pyrrole molecules because of the negative adsorption energy. But it is unlikely to be entirely correct because, from the preparation point of view, the amount of Si necessary for the formation of this structure seems to be too high.

## ACKNOWLEDGMENTS

Grants of computer time from the Leibniz-Rechenzentrum München and the Höchstleistungs-Rechenzentrum Stuttgart are gratefully acknowledged. We thank the Deutsche Forschungsgemeinschaft for financial support (Grant No. SCHM-1361/6-2) We also acknowledge support from the EU network of Excellence NANOQUANTA (Grant No. NMP4-CT-2004-500198).

*Electronic address: preuss@ifto.physik.uni-jena.de

[1] R. J. Hamers, Nature (London) **412**, 489 (2001).
[2] R. A. Wolkow, Annu. Rev. Phys. Chem. **50**, 413 (1999).
[3] M. A. Filler and S. F. Bent, Prog. Surf. Sci. **73**, 1 (2003).
[4] D. Williams, Med. Device Technol. **14**, 10 (2003).
[5] P. Käckell, J. Furthmüller, and F. Bechstedt, Phys. Rev. B **60**, 13261 (1999).
[6] D. Nakamura, I. Gunjishima, S. Yamaguchi, T. Ito, A. Okamoto, H. Kondo, S. Onda, and K. Takatori, Nature (London) **430**, 1009 (2004).
[7] K. Seino, W. G. Schmidt, M. Preuss, and F. Bechstedt, J. Phys. Chem. B **107**, 5031 (2003).
[8] B. Schröter, K. Komlev, and W. Richter, Mater. Sci. Eng., B **88**, 259 (2002).
[9] A. Winkelmann, B. Schröter, and W. Richter, J. Phys.: Condens. Matter **16**, S1555 (2004).
[10] J. P. Perdew, J. A. Chevary, S. H. Vosko, K. A. Jackson, M. R. Pederson, D. J. Singh, and C. Fiolhais, Phys. Rev. B **46**, 6671 (1992).
[11] G. Kresse and J. Furthmüller, Comput. Mater. Sci. **6**, 15 (1996).
[12] G. Kresse and D. Joubert, Phys. Rev. B **59**, 1758 (1999).
[13] M. Preuss, W. G. Schmidt, K. Seino, J. Furthmüller, and F. Bechstedt, J. Comput. Chem. **25**, 112 (2004).
[14] K. Seino, W. G. Schmidt, J. Furthmüller, and F. Bechstedt, Phys. Rev. B **66**, 235323 (2002).
[15] M. Preuss, W. G. Schmidt, K. Seino, and F. Bechstedt, Appl. Surf. Sci. **234**, 155 (2004).
[16] M. Preuss and F. Bechstedt, Phys. Rev. B **73**, 155413 (2006).
[17] F. Bechstedt, P. Käckell, A. Zywietz, K. Karch, B. Adolph, K. Tenelsen, and J. Furthmüller, Phys. Status Solidi B **202**, 35 (1997).
[18] P. Käckell, J. Furthmüller, and F. Bechstedt, Diamond Relat. Mater. **6**, 1346 (1997).
[19] P. Pulay, Chem. Phys. Lett. **73**, 393 (1980).
[20] D. M. Wood and A. Zunger, J. Phys. A **18**, 1343 (1985).
[21] S. Lizzit *et al.*, Phys. Rev. B **63**, 205419 (2001).
[22] T. Koopmans, Physica (Amsterdam) **1**, 104 (1934).
[23] L. Köhler and G. Kresse, Phys. Rev. B **70**, 165405 (2004).
[24] M. Gajdoš, A. Eichler, and J. Hafner, Surf. Sci. **531**, 272 (2003).
[25] R. Chen, J. Mater. Sci. **11**, 1521 (1976).
[26] H.-J. Butt, K. Graf, and M. Kappl, *Physics and Chemistry of Interfaces* (Wiley-VCH, 2003).
[27] J. J. Randall and M. H. F. Wilkins, Proc. R. Soc. London, Ser. A **366**, 390 (1945).
[28] M. Sabisch, P. Krüger, and J. Pollmann, Phys. Rev. B **55**, 10561 (1997).
[29] J. Furthmüller, F. Bechstedt, H. Hüsken, B. Schröter, and W. Richter, Phys. Rev. B **58**, 13712 (1998).
[30] J. Furthmüller, P. Käckell, F. Bechstedt, A. Fissel, K. Pfennighaus, B. Schröter, and W. Richter, J. Electron. Mater. **27**, 848 (1998).
[31] U. Starke, J. Schardt, J. Bernhardt, M. Franke, K. Reuter, H. Wedler, K. Heinz, J. Furthmüller, P. Käckell, and F. Bechstedt, Phys. Rev. Lett. **80**, 758 (1998).
[32] L. I. Johansson, P.-A. Glans, and N. Hellgren, Surf. Sci. **405**, 288 (1998).
[33] S. Nakanishi, H. Tokutaka, K. Nishimori, S. Kishida, and N. Ishihara, Appl. Surf. Sci. **41**, 44 (1989).
[34] M. Hollering, J. Bernhardt, J. Schardt, A. Ziegler, R. Graupner, B. Mattern, A. P. J. Stampfl, U. Starke, K. Heinz, and L. Ley, Phys. Rev. B **58**, 4992 (1998).
[35] I. Forbeaux, J.-M. Themlin, A. Charrier, F. Thibaudau, and J.-M. Debever, Appl. Surf. Sci. **162**, 406 (2000).
[36] U. Starke, Mater. Sci. Forum **353**, 205 (2001).
[37] H. E. Hoster, M. A. Kulakov, and B. Bullemer, Surf. Sci. **382**, L658 (1997).
[38] L. Li and I. S. T. Tsong, Surf. Sci. **351**, 141 (1996).
[39] G.-X. Qian, R. M. Martin, and D. J. Chadi, Phys. Rev. B **38**, 7649 (1988).
[40] W. G. Schmidt, P. Käckell, and F. Bechstedt, Surf. Sci. **357–358**, 545 (1996).